



Strength Reduction of Initial High-Stress Rock Pillars Under Different Triaxial Unloading Paths

Wuxing Wu^{1,2} · Fengqiang Gong^{1,2,3} · Quan Jiang³ · Lei He²

Received: 2 July 2022 / Accepted: 8 January 2023 / Published online: 26 January 2023
© The Author(s), under exclusive licence to Springer-Verlag GmbH Austria, part of Springer Nature 2023

Abstract

The mechanical behavior of deep rock pillars is closely related to the coupling effect of the initial high stress and the excavation-unloading process. In this study, the failure and strength characteristics of rock pillars are studied under triaxial unloading paths of three-dimensional (3D) initial high stress followed by two-dimensional (2D) stress unloading and one-dimensional (1D) stress adjustment. Two different 2D stress unloading paths were used: horizontal bidirectional sequential unloading path (YU test), and horizontal bidirectional simultaneous unloading path (TU test). The 3D initial high stresses were $\sigma_1 = 60$ MPa, $\sigma_2 = \sigma_3 = 10, 20, 30, 40,$ and 50 MPa, that were applied on cubic granite specimens ($50 \times 50 \times 50$ mm). Uniaxial compression tests are also conducted for comparison. Violent rockburst occurred in all specimens under the triaxial unloading paths. The results reveal that the peak strengths of the cubic granite specimens under the triaxial unloading paths are significantly lower than the uniaxial compressive strength, namely exhibiting a remarkable strength reduction effect, and the degree of strength reduction will increase with the increase of initial stress. Further, the specimen strengths in the TU tests are lower than those in the YU tests, which indicates that the weakening intensity effect of simultaneous unloading is greater than that of sequential unloading. The weakening mechanism of deep pillar under high-stress unloading can be expressed as that the 3D initial stress determines the strength level of the pillar, whereas the triaxial unloading path affects its weakening intensity.

Highlights

- The rockburst failure and strength characteristics of rock pillars under the high-stress condition were studied from the perspective of triaxial unloading of 3D initial high stress + 2D stress unloading + 1D stress adjustment.
- The pillar strength reduction effect was observed and the triaxial unloading path has a significant influence on the strength reduction effect.
- The initial 3D stress determines the strength level of the pillar, whereas the triaxial unloading path affects its weakening intensity.

✉ Fengqiang Gong
fengqiangg@126.com

¹ Engineering Research Center of Safety and Protection of Explosion & Impact of Ministry of Education (ERCSP EIME), Southeast University, Nanjing 211189, China

² School of Civil Engineering, Southeast University, Nanjing 211189, China

³ State Key Laboratory of Geomechanics and Geotechnical Engineering, Institute of Rock and Soil Mechanics, Chinese Academy of Sciences, Wuhan 430071, China

Keywords Rock pillar · Deep pillar failure · Rockburst · Strength-reduction effect · Triaxial unloading paths · High-stress unloading

Abbreviations

3D	Three-dimensional
2D	Two-dimensional
1D	One-dimensional
YU	Horizontal bidirectional sequential unloading path
TU	Horizontal bidirectional simultaneous unloading path
UC	Uniaxial compression test
UCS	Uniaxial compressive strength
SWR	Strength-weakening rate

List of Symbols

σ_1	Maximum principal stress
σ_2	Intermediate principal stress
σ_3	Minimum principal stress
σ_x	X-Directional stress
σ_y	Y-Directional stress
σ_{YU}	Peak strength of horizontal bidirectional sequential unloading path test
σ_{TU}	Peak strength of horizontal bidirectional simultaneous unloading path test
t	Shear failure strength
c	Cohesion
φ	Internal friction angle
σ_{TUS}	Triaxial compress strength
σ_{UCS}	Uniaxial compressive strength

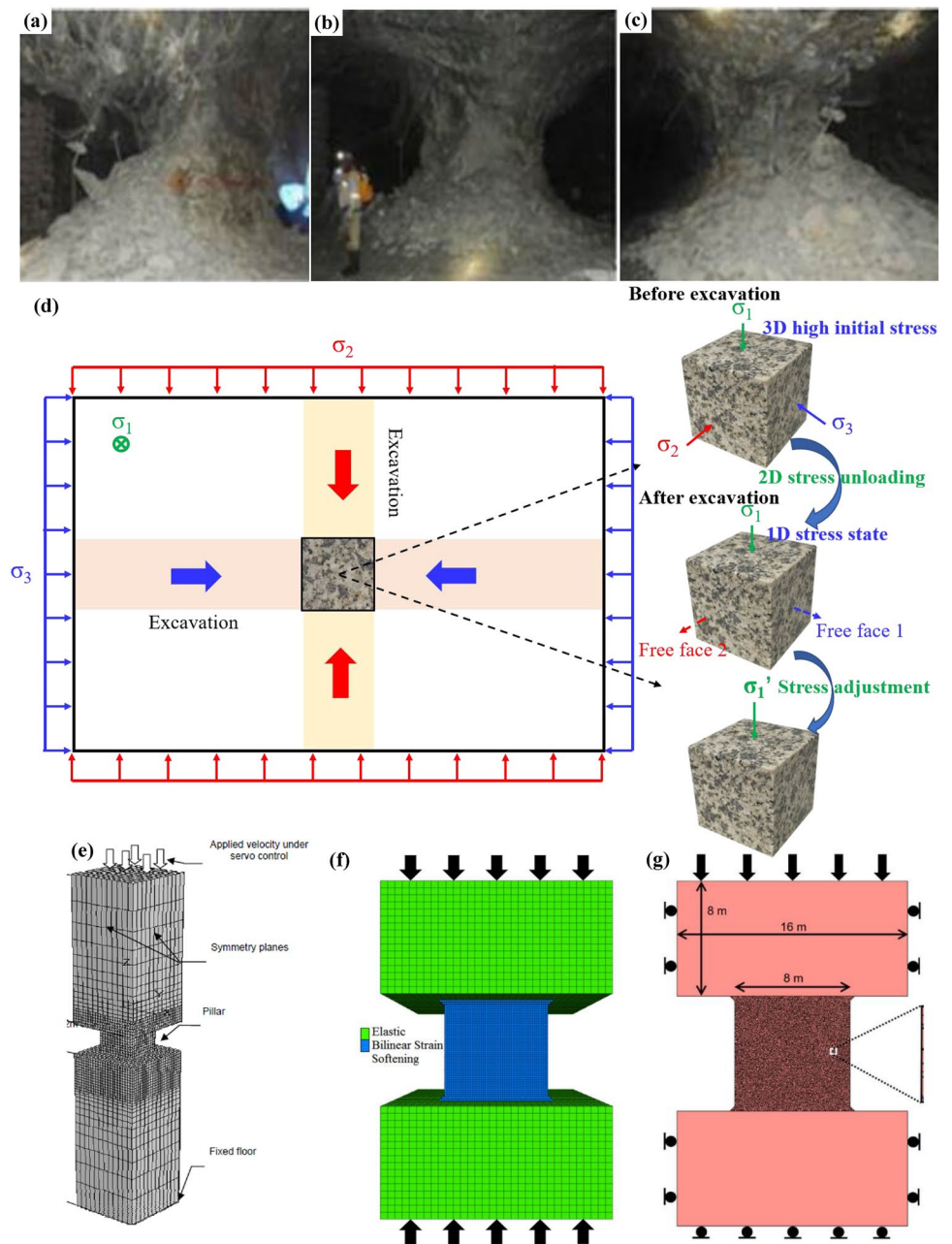
1 Introduction

Rock pillars under high stress are common in deep mines, wherein they are used to maintain the stability of underground engineering excavations (Cording et al. 2015; Renani and Martin 2018; Wang and Cai 2021). Constructions in deep mines inevitably involve excavation-unloading processes, which frequently induce rock brittle failure, such as spalling and rockburst, and lead to major safety hazards on-site (Ortlepp and Stacey 1994; Martin 1997; Martin et al. 2003; Zhang et al. 2012). Moreover, estimating rock pillar strength under high stress is very important for deep mines construction; however, evaluating pillar strength is highly challenging owing to several factors, including the in situ stress, excavation-unloading method, and rock mass quality (Sengani 2018; Martin and Maybee 2000; Esterguizen et al. 2011). Figure 1a–c shows the characteristics of rock pillar failure in deep mines on-site (Sengani 2018). Understandably, a pillar failure disaster makes stability in deep mines highly challenging. In addition, rock pillar failure and strength characteristics are related to the changes in the stress state before and after the excavation process (Martin

and Maybee 2000). However, literature on rock pillar failure and strength analysis from the perspective of a high-stress unloading path is scarce. Such a path refers to a deep rock in a three-dimensional (3D) initial high stress before the excavation-unloading process. Under this condition, the formation of a rock pillar is similar to two-dimensional (2D) stress unloading, and the rock pillar is subject to a stress adjustment caused by the stress redistribution, which induces pillar failure. Figure 1d shows a schematic of an entire stress path during the unloading process of rock pillar excavation, and the high-stress unloading path is summarized as “3D initial high stress + 2D stress unloading + stress adjustment”. Figure 1e–g shows schematics of the high-stress rock pillar in a 1D stress state after excavation unloading, respectively (Sinha and Walton 2021a; Sankhanee and Walton 2018; Li et al. 2019). However, recently, few related studies have been conducted; thus, the innovation of this study is investigating the failure characteristics and strength reduction of the high-stress rock pillar caused by a high-stress unloading path: 3D initial high stress + 2D stress unloading + 1D stress adjustment.

Until now, research on deep mining engineering has typically been prominent, and abundant results have been obtained. Research on rock failure characteristics under excavation unloading focuses primarily on true triaxial tests (He et al. 2021; Jiang et al. 2021; Si and Gong 2020; Li et al. 2017; Liu et al. 2021; Zhao and Cai 2015). Si and Gong (2020) conducted a true triaxial unloading test on a cubic granite specimen. After confining pressure unloading, the specimen suffered severe rockburst failure under stress adjustment and the failure mode of the specimen changed. He et al. (2021) used self-developed true triaxial equipment to conduct an experimental study on the strain rockburst characteristics of sandstone under true triaxial loading and double-face unloading in one direction. In addition, considerable research has been performed to consider the effect of stress adjustment on rockburst (Cai 2008a, b; He et al. 2014; Hu et al. 2019; Gong et al. 2018, 2023; Luo et al. 2019; Wu et al. 2020). He et al. (2014) conducted true triaxial compression tests on prefabricated hole specimens by simulating the sidewall rockburst failure process under vertical stress adjustment after excavation. Accordingly, they conducted numerous true triaxial compression tests on prefabricated specimens and systematically explored the sidewall failure characteristics under stress adjustment after excavation unloading. However, the abovementioned tests considered only the effect of triaxial unloading or stress adjustment on rock failure under a single factor, and most of them simulated sidewall failure, whereas there are very few studies on rock pillars.

Fig. 1 Rock pillar failure: **a–c** rock pillar failure on-site (Sengani 2018); **d** schematic of entire stress path of rock pillar; **e–g** schematics of rock pillar bearing stress after excavation and unloading (Sinha and Walton 2021a; Sankhane and Walton 2018; Li et al. 2019)



At present, although studies on pillar failure and strength considering triaxial unloading and stress environment are relatively few, relevant research has not stagnated. Regarding pillar failure, studies primarily consider pillar failure characteristics under loading conditions (Li et al. 2007; Gong et al. 2010; Xu et al. 2012; Deng et al. 2019; Deng 2021). Li et al. (2007) examined the mechanical response mechanism of the rockburst failure under the dynamic disturbance of a high pre-static pillar after excavation by performing numerical simulations. Similarly, Gong et al. (2010) conducted 1D coupled static–dynamic tests to analyze the energy evolution characteristics of pillar rockburst instability and founded the

“Energy release” indoor rockburst phenomenon during sandstone specimen failure. In addition, Huang et al. (2017) theoretically derived the basic mechanical properties required for pillar rockburst. Furthermore, pillar strength is critical to the long-term stability of underground engineering (Esterhuizen 2006; Chen et al. 2009; Kaiser et al. 2011; Sankhane and Walton 2018; Li et al. 2019; Sinha and Walton 2021b). Wang and Cai (2021) established a numerical model of the strength and deformation of rock pillars subjected to time-dependent and analyzed the long-term stability of a rock pillar. Sankhane and Walton (2018) focused on studying the progressive S-shaped strength criterion and demonstrated its

ability to reproduce observed pillar behavior. Li et al. (2019) used finite discrete element models to study rock pillar failure behavior in laboratory and in situ scales. They found that the post-yield behavior obtained from rock pillar models using laboratory parameters was more brittle than expected in practice. In summary, the abovementioned research on pillar failure and strength characteristics is limited to the loading condition, and the influence of an entire stress path (Fig. 1d) on the stability of the rock pillar is basically not considered.

In this study, rock pillar failure and strength characteristics were investigated under triaxial unloading paths of 3D initial high stress followed by 2D stress unloading and 1D stress adjustment. Two different 2D stress unloading paths were used: horizontal bidirectional sequential unloading path (YU test), and horizontal bidirectional simultaneous unloading path (TU test). The 3D initial high stresses ($\sigma_1 = 60$ MPa, $\sigma_2 = \sigma_3 = 10, 20, 30, 40,$ and 50 MPa) were applied to cubic granite specimens ($50 \times 50 \times 50$ mm). Additionally, uniaxial compression (UC) tests were performed for comparison. The peak strength, rockburst failure process, and failure model were obtained and compared. Finally, the mechanical behavior of the deep rock pillar under the triaxial unloading paths was examined based on the test results.

2 Experimental Procedures

2.1 Mechanical Properties and Preparation of Zhumadian Granite

Rock pillar failure tests under different unloading paths of high stresses were performed on a fine-grained homogeneous Zhumadian granite (Henan Province, China). Optical analyses of thin sections of the granite using the polarizing microscope to determine the mineral composition and structure, and the results are shown in Fig. 2a and b. It can

be observed that the granite has a blocky structure without remarkable defects, and that the average mineral particle size is approximately 0.2–0.3 mm. The petrographic studies according to Fig. 2c reveals that the Zhumadian granite is composed primarily of quartz (33%), K-feldspar (32%), plagioclase (30%), biotite (3%), and other minerals (2%).

All standard cubic specimens of size $50 \times 50 \times 50$ mm used in the triaxial unloading path tests were cored from the same Zhumadian granite block in the same direction to reduce the influence of anisotropy, as illustrated in Fig. 3a. The blocks were carefully polished to reduce the influence of dimensional errors, where the dimensional tolerance of all end faces was controlled within 50 ± 0.0025 mm and their perpendicularity tolerance was 0.025 mm (Feng et al. 2019). The stress–strain curves and typical failure modes of the cubic specimens under UC tests are shown in Fig. 3b and c. In the process of uniaxial compression failure of the cube specimens, they emitted loud sound accompanied by violent rockburst characteristics, such as rock fragments ejecting, which was similar to the failure characteristics of cylinder specimen under uniaxial compression (Wu et al. 2022). The average UC strength (UCS) of each cubic specimen was 140.00 ± 0.45 MPa, and the UC failure mode was tension splitting. Additionally, each cubic specimen had a density of 2600.52 ± 2.79 kg/cm³, P-wave velocity of 3879.18 ± 74.64 m/s, Young's modulus of 40.48 ± 1.35 GPa, and indirect tensile strength of 7.50 ± 0.04 MPa.

2.2 Testing Apparatus

As shown in Fig. 4, the rock pillar failure tests under different triaxial unloading paths were performed on a true triaxial testing system, which comprised a data acquisition system and independent loading and unloading units in the X-, Y-, and Z-directions. The true triaxial equipment has high stiffness, in which the horizontal and vertical loading frame stiffness is 400 kN/mm and 1000 kN/mm,

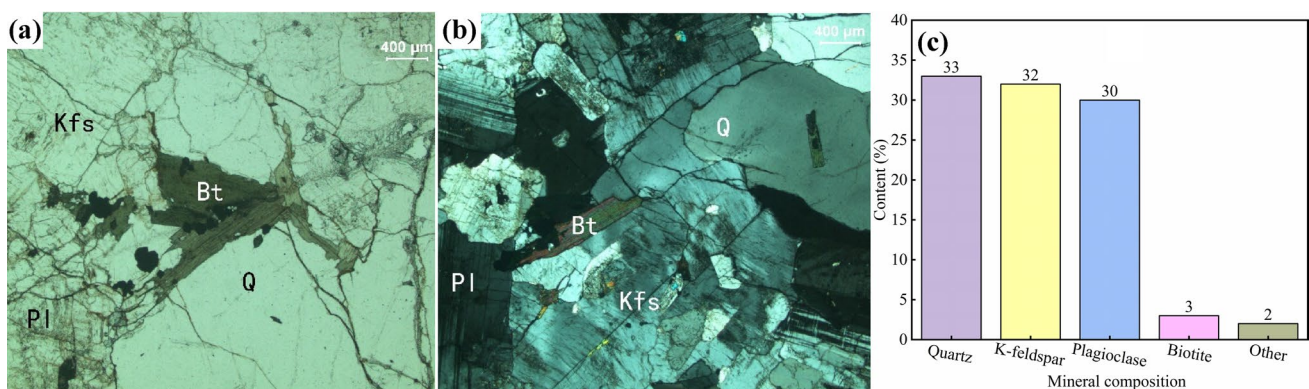


Fig. 2 Thin-section observation of granite material (Wu et al. 2022): a single and b orthogonally polarized light; c mineral composition

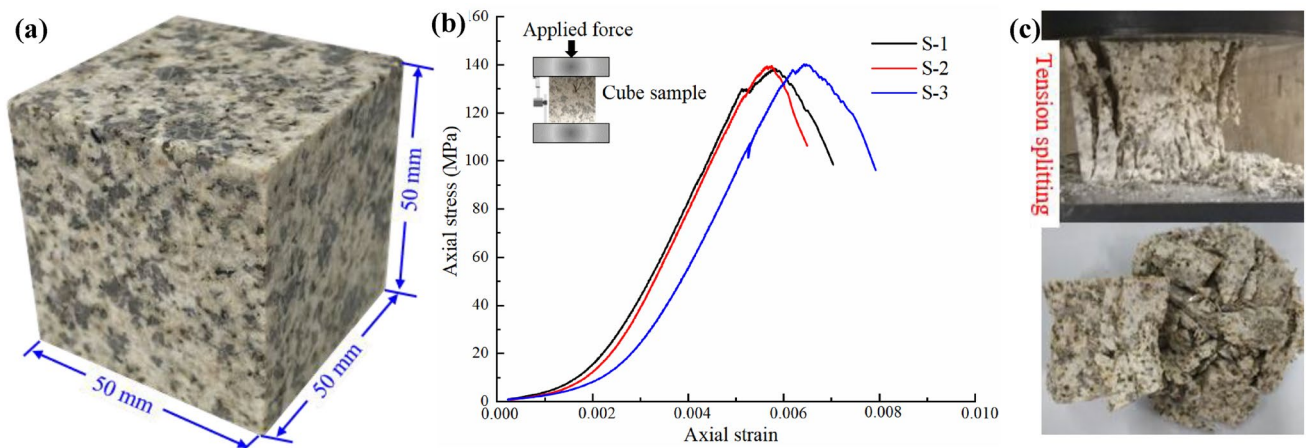


Fig. 3 Basic information of cubic sample: **a** specimen geometry; **b** and **c** typical static axial stress–strain curves and corresponding rockburst failure characteristics

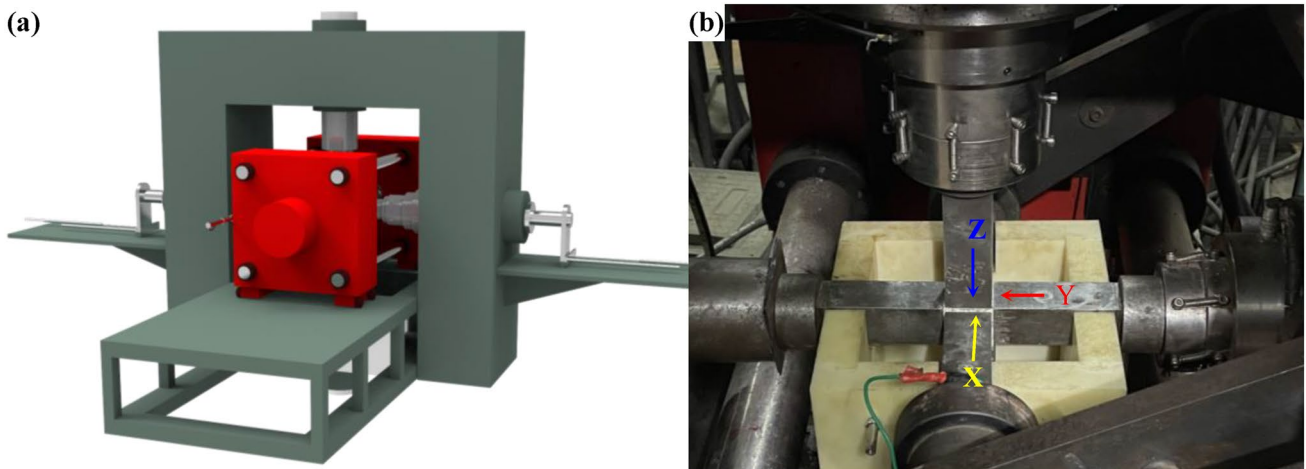


Fig. 4 Test equipment: **a** triaxial system; **b** corresponding 3D stress loading chamber

respectively, belonging to the rigid testing machine. The maximum load capacity in X - and Y -directions is 2000 kN, whereas that in the Z -direction is 3000 kN, and the loading rate of force is 10 N/s–10 kN/s. In the displacement aspect, the measurement range is 0–200 mm in the X -direction, and 0–100 mm in the Y - and Z -directions. The measurement accuracy in all three directions was $< \pm 0.5\%$ and the resolution was 0.001 mm. The deformation measurement range was 0–10 mm, with a measuring accuracy of $< \pm 0.5\%$ and a resolution of 0.0005 mm. The micro-camera captures and records video at a sampling rate of 30 frames per second, and the image resolution is set to 160×120 pixels. More details about the test system can be found in the references Gong et al. (2018).

2.3 2D Unloading Path Design

It is well known that excavation unloading changes the stress state of the rock and induces stress redistribution, which is also affected by the stress unloading path. Therefore, the stress change process of the rock pillar in deep mining engineering occurs in a 3D initial high stress state followed by excavation unloading and 1D stress adjustment. This entire stress change process can be summarized as 3D initial high stress + 2D stress unloading + 1D stress adjustment. A 2D stress unloading process of a rock pillar (Fig. 1d) can be divided into sequential and simultaneous unloading paths in the horizontal bidirectional. Thus, rock pillar failure processes were conducted under two triaxial unloading paths on the triaxial testing system. As illustrated in Figs. 5 and 6,

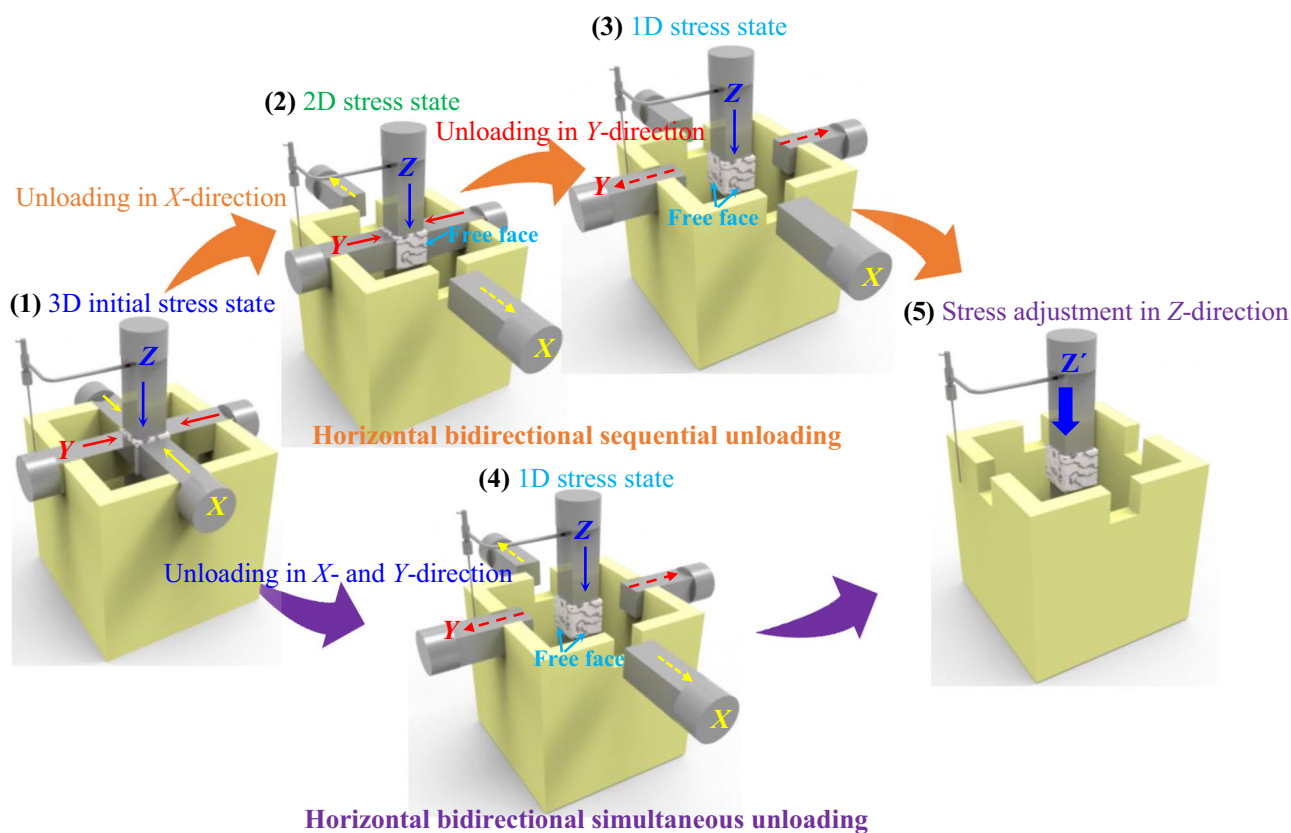


Fig. 5 Schematic of 3D stress state unloading to 1D stress state under two different modes: (1)→(2)→(3)→(5) represents YU test and (1)→(4)→(5) depicts TU test

these are horizontal bidirectional sequential and simultaneous unloading tests (YU and TU tests, respectively). Table 1 lists the cubic granite specimen labels for the two triaxial unloading paths. In order to eliminate the end effect as much as possible, we applied a lot of lubricant between the rock specimen and the loading platens, but it may not be possible to completely eliminate the end effect. The detailed test process was as follows.

2.3.1 (1) YU Test

In Fig. 5, steps (1)→(2)→(3)→(5) schematically show the triaxial unloading path by which the YU tests were conducted on the triaxial system, and the corresponding stress paths are shown in Fig. 6a. In the 3D initial stress loading stage, the three directions (X, Y, Z) were loaded with the preset values at a loading rate of 0.4 MPa/s and subsequently maintained for 5 min (step (1) in Fig. 5). Note that the X- and Y-directions were subjected to equal confining pressure loading, and the preset confining pressures were 10, 20, 30, 40, and 50 MPa, respectively, whereas the preset threshold in the Z-direction was

60 MPa. Subsequently, the loading in Y- and Z-directions was kept unchanged and the X-direction was unloaded to 0 MPa at an unloading rate of 1.0 MPa/s, which was maintained for 2 min (step (2) in Fig. 5). Following this, the same unloading process was performed in the Y-direction, wherein the specimen was subjected to stress only in the Z-direction, and the specimen was in a 1D stress state (step (3) in Fig. 5). Finally, the Z-direction stress was activated again and increased at a loading rate of 0.4 MPa/s until the specimen failed (step (5) in Fig. 5).

2.3.2 (2) Tu Test

In Fig. 5, steps (1)→(4)→(5) schematically show the entire process by which the TU tests are conducted on the triaxial system, and the corresponding stress paths are shown in Fig. 6b. Noticeably, although steps (1) and (5) are the same as in the YU tests, there are significant differences in the 2D stress unloading process. Specifically, the horizontal X- and Y-directions were simultaneously unloaded to 0 MPa at a rate of 1.0 MPa/s in the TU tests (step (4) in Fig. 5).

Fig. 6 Schematics of high-stress unloading path: **a** YU and **b** TU tests (σ_1 , σ_2 , and σ_3 represent X-, Y- and Z-direction stresses, respectively)

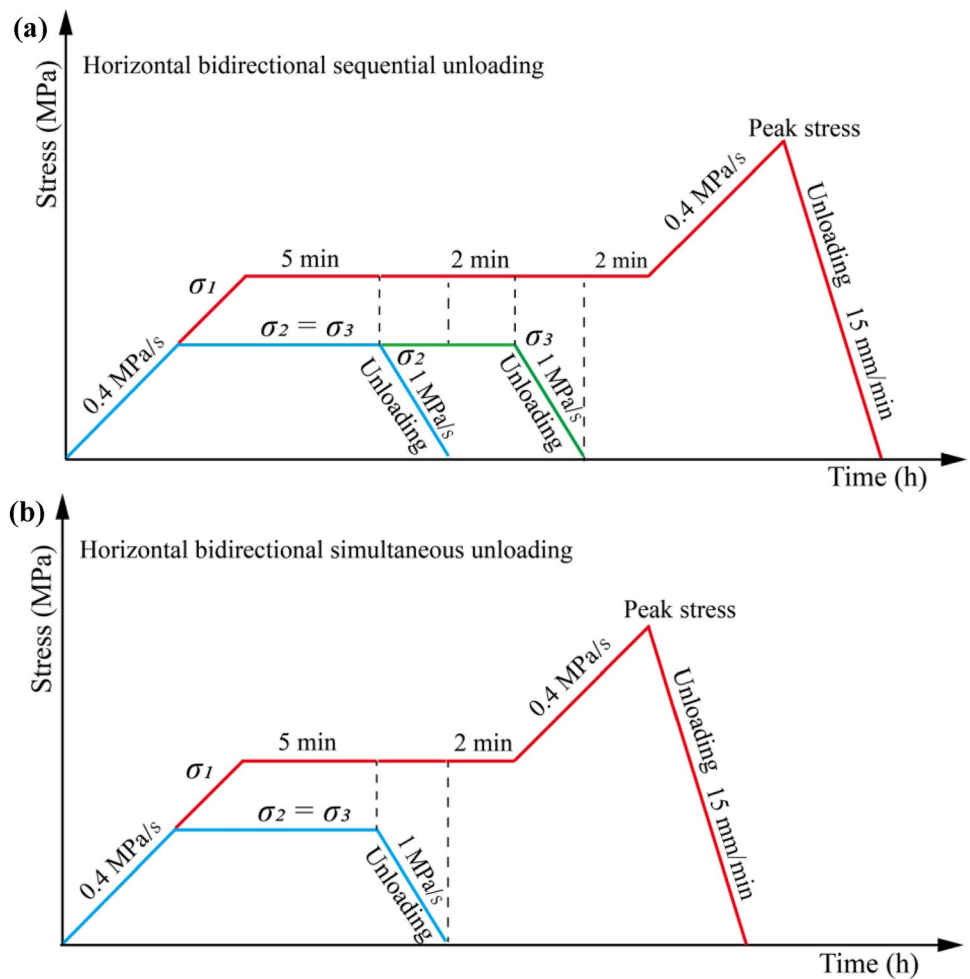


Table 1 Different types of tests

Test types	3D initial stress			2D stress unloading			1D stress state	Sample ID
	σ_1 /MPa	σ_2 /MPa	σ_3 /MPa	σ_1 /MPa	σ_2 /MPa	σ_3 /MPa	σ_1 /MPa	
YU test	60	10	10	60	10 → 0 ^a	10 → 0 ^b	60	YU-10
	60	20	20	60	20 → 0 ^a	20 → 0 ^b	60	YU-20
	60	30	30	60	30 → 0 ^a	30 → 0 ^b	60	YU-30
	60	40	40	60	40 → 0 ^a	40 → 0 ^b	60	YU-40
	60	50	50	60	50 → 0 ^a	50 → 0 ^b	60	YU-50
TU test	60	10	10	60	10 → 0*		60	TU-10
	60	20	20	60	20 → 0*		60	TU-20
	60	30	30	60	30 → 0*		60	TU-30
	60	40	40	60	40 → 0*		60	TU-40
	60	50	50	60	50 → 0*		60	TU-50

^a represents unloading first in X-direction, ^b represents unloading later in Y-direction, * represents simultaneous unloading in X- and Y-directions

3 Results and Analysis

A series of triaxial unloading path tests of “3D initial high stress + 2D stress unloading + 1D stress adjustment” was performed to reproduce the rock pillar failure. This section focuses on the stress characteristics, pillar rockburst failure process, and pillar strength-reduction effect (also known as strength-weakening effect) under the triaxial unloading path.

3.1 Stress Characteristics of Rock Pillar Under Triaxial Unloading Path

The stress–time and stress–strain curves can reflect the actual stress–loading paths and deformation characteristics of the cubic granite specimens in the triaxial unloading tests, respectively, as shown in Fig. 7. Figure 7a–d depict the typical stress–time and stress–strain in the three directions of cubic granite specimens YU-10 and TU-30. Figure 7e and f show the Z-direction stress–strain characteristics of all cubic granite specimens in the YU and TU tests. Figure 7a and c show that two triaxial unloading tests are conducted in strict compliance with the test scheme in Fig. 6. Noticeably, the Z-direction stress–strain curves of all cubic granite specimens can be divided into compaction, elastic, inelastic, and failure segments (seen in Fig. 7e and f). In comparison, those of the X- and Y-directions show compression, elastic, and unloading segments (seen in Fig. 7b and d). Additionally, stresses were not constrained in the X- and Y-directions after the 2D stress unloading, whereas the Z-direction stress remained unchanged; therefore, a notable stress step was observed in the Z-direction owing to the Poisson effect. Moreover, remarkable stress hysteresis loops were formed in X- and Y-directions, and the corresponding strains did not return to the original values, which suggests that the 2D stress unloading induced notable local damage in a rock pillar specimen. Therefore, compared to the stress–strain curves obtained under UC tests (Fig. 3b), those from the YU and TU tests present a distinct yield segment near the peak strength owing to the unloading effect (Fig. 7e and f). This suggests that the mechanical properties of a rock pillar specimen are affected by the unloading effect, such as plastic enhancement and brittleness reduction. It can be concluded that the mechanical behavior of the cubic granite specimens under “3D initial stress + 2D stress unloading + 1D stress adjustment” becomes more complex. In summary, the mechanical characteristics of a rock pillar specimen under the considered triaxial unloading paths are essentially different from those under uniaxial loading, i.e., the physical characteristics of rock pillar are changed under triaxial unloading.

3.2 Rockburst Failure Process of Rock Pillar Under Triaxial Unloading Path

During the 2D stress unloading process, no remarkable macroscopic damage was caused to the cubic granite specimen surface, and it remained intact, due to the axial load being below the UCS. However, the axial strain will increase and the stress step appears in Fig. 7, which indicates that the triaxial unloading causes a certain degree of damage to the specimen. This indicates that the triaxial unloading did not immediately induce rock pillar macroscopic failure until the external stress was adjusted to the maximum bearing capacity of the cubic granite specimen. Figures 8 and 9 illustrate the severe dynamic rockburst failure abruptly occurred as the Z-direction stress was adjusted to the maximum bearing capacity of the cubic granite specimen. The triaxial unloading paths did not seem to significantly affect the rockburst failure characteristics of the cubic granite specimens, which reflects that the rockburst failure processes in the YU and TU tests are very similar. Due to the narrow inside of the true triaxial apparatus, it is impossible to obtain the range and distance of rock bursting, which leads to the inability to reflect the intensity of rockburst. In the YU and TU tests, with increase in the Z-direction stress, remarkable macroscopic cracks were first observed on the surfaces of the cubic granite specimens (Figs. 8a₁–e₁ and 9a₁–e₁). After 0.04 s, numerous fine and dust particles were ejected on the surface and accompanied by a high noise; after 0.08 s, the damage phenomenon intensified, and increasing number of fine particles and rock flakes were ejected. After 0.12 s, the surface ejection phenomenon became slightly gradual, but new fine particles and rock flakes were still observed to fly out. The duration of the dynamic rockburst failure progress of all specimens was very short. The yield stages of the stress–strain curves under the unloading confining pressure of 50 MPa were very significant, and the strain increased rapidly under the extremely small stress change (Fig. 7). This reflects an increase in the plasticity of the rock specimen and a decrease in the brittleness. This demonstrates that the confining pressure unloading may affect the rockburst intensity, particularly the high-confining pressure unloading. It also suggests that the triaxial unloading affects its mechanical characteristics of deep rock pillar.

3.3 Post-peak Failure Mode of Rock Pillar

Understanding the post-peak failure mode of the rock is helpful in analyzing the failure mechanism (Kate and Reches 2004). Figure 10 shows the post-peak failure characteristics of the cubic granite specimens obtained in the UC, YU, and TU tests, respectively. Figure 10a presents the post-peak failure characteristics of the

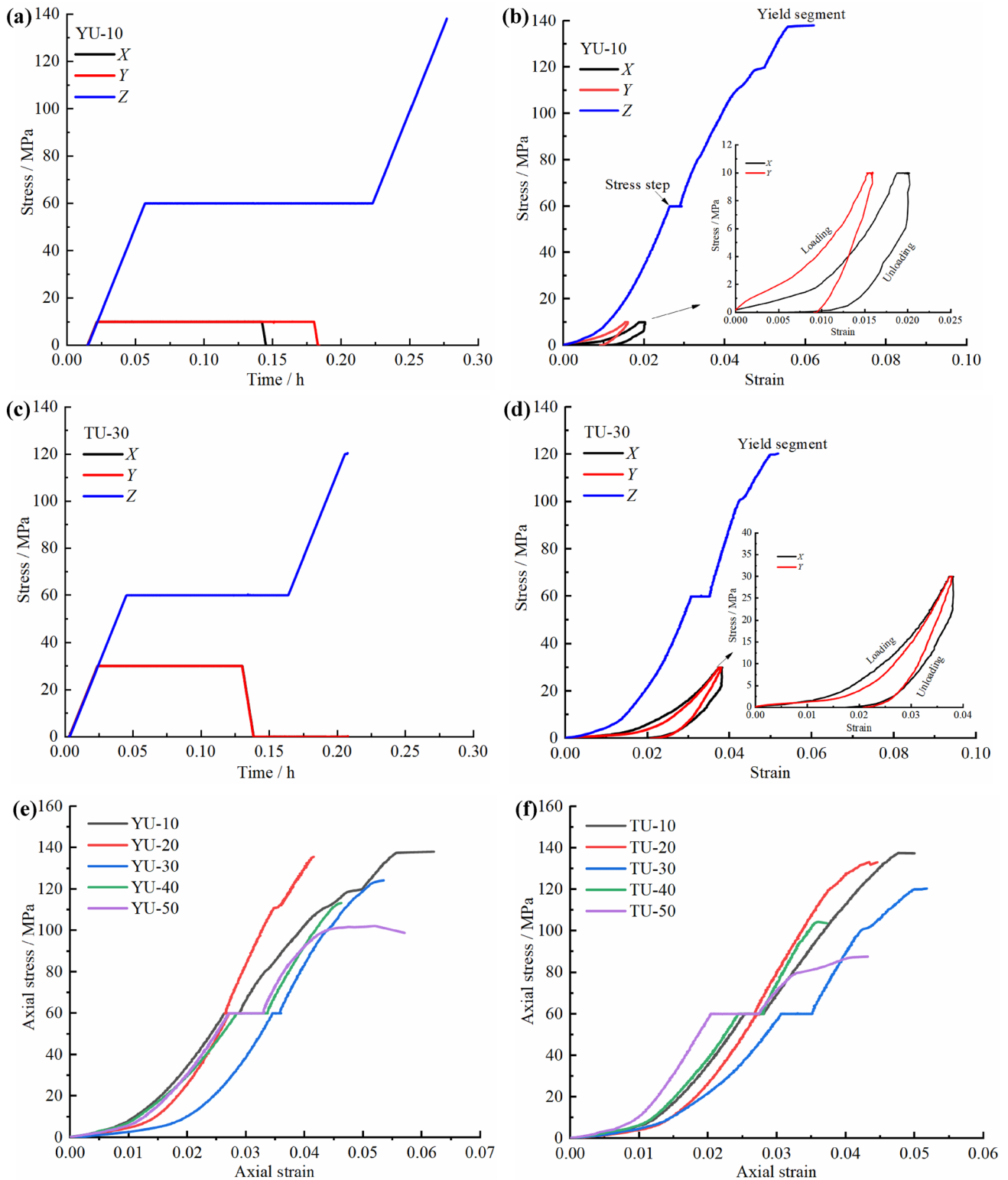


Fig. 7 Stress characteristics of samples under different high-stress unloading paths: **a** and **b** stress–time and stress–strain curves of specimen YU-10; **c** and **d** stress–time and stress–strain curves of specimen TU-30; **e** and **f** Z-direction stress–strain curves from YU and TU tests



Fig. 8 Rockburst failure process in YU test

cubic granite specimens in the UC tests, primarily in the tension-splitting failure mode, and it shows that all specimens remained basically intact. In the YU tests, the shear failure mode was the main mode under low-confining pressure unloading (Fig. 10b₁ and b₂), and the shear–tension failure mode dominated as the confining pressure increased (Fig. 10b₃ and b₄), which is similar to the failure mode of surrounding rock after deep mining unloading (Li 2021). Similarly, the shear–tension failure mode was dominant in the TU tests (Fig. 10c). Furthermore, Wang and Cai (2021) reproduced the shear failure characteristics of a rock pillar by numerical simulations in combination with field engineering cases, and results

are shown in Fig. 11a. Sankhane and Walton (2018) also concluded that the failure mode of a rock pillar is mainly shear failure, which is shown in Fig. 11b. The failure mode of a rock pillar under the high-stress triaxial unloading path simulated in this study is in agreement with these conclusions, which shows that the simulation tests are reliable. Although two triaxial unloading stress paths do not significantly affect the failure modes of cubic granite specimens, the strength-reduction effect directly indicates that the unloading path has a very significant influence on the strength characteristics of the rock specimens (Fig. 7). Compared with the UC test, triaxial unloading changes the failure mode of the cubic granite specimens;

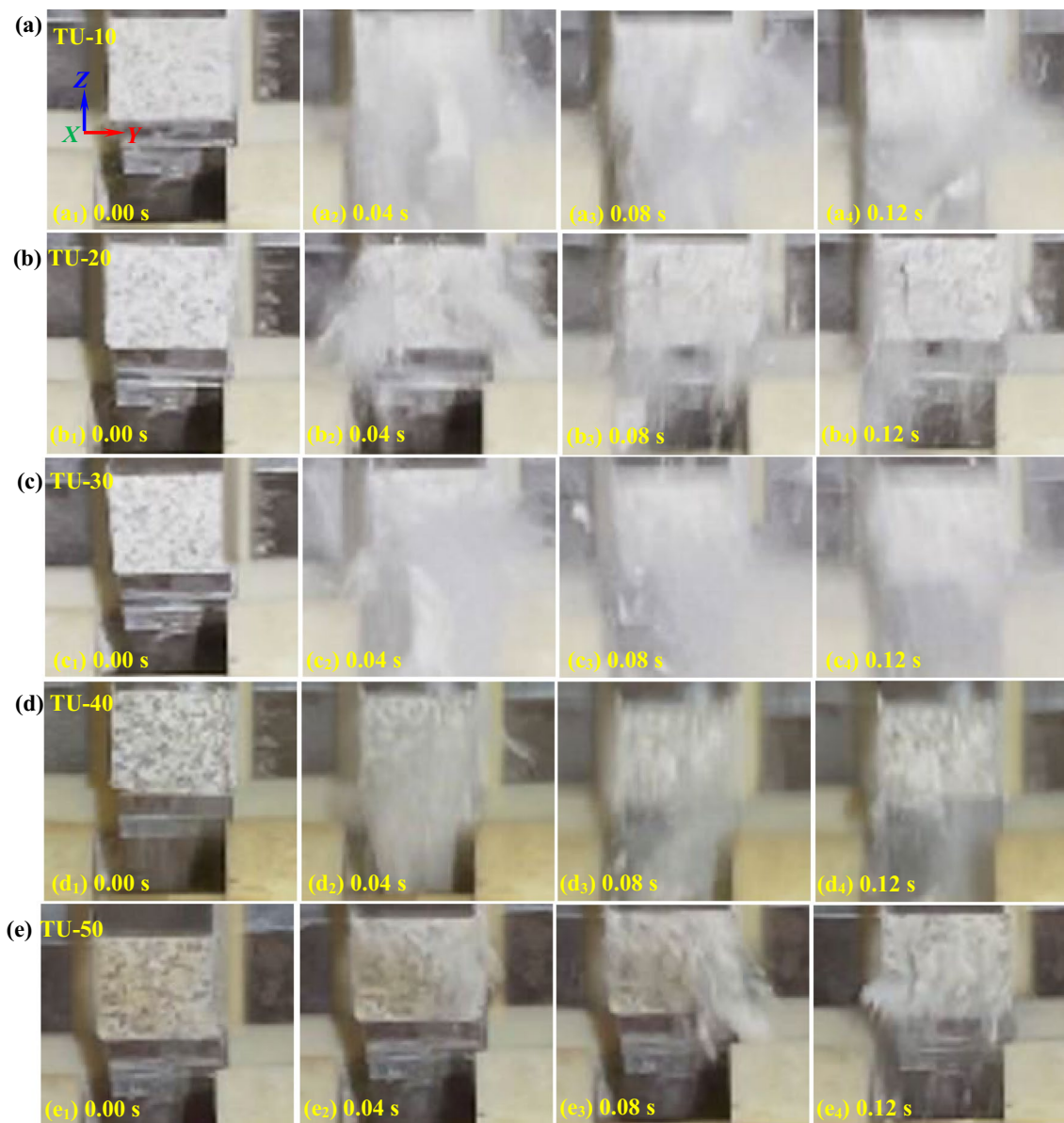


Fig. 9 Rockburst failure process in TU test

additionally, the unloading path and confining pressure affect the failure mode.

3.4 Strength-Reduction Effect of Rock Pillar Under Triaxial Unloading Path

Table 2 lists the peak strength values of the cubic granite specimens obtained from two triaxial high-stress unloading path tests. Compared to the *UCS*, the peak strengths of the cubic granite specimens under the “3D initial high stress + 2D stress unloading + 1D stress adjustment” stress path was significantly reduced, and they were affected by

the triaxial unloading path. The peak strengths of all cubic granite specimens were lower than those of the *UCS*, and the peak strengths significantly decreased with increase in the confining pressure, regardless of the unloading effect. This is observed from Fig. 12a. In the YU tests, with increase in the confining pressure, the peak strengths of cubic granite specimens ranged between 138.07 and 102.22 MPa, and compared to the uniaxial compressive strength (i.e., $UCS = 140.00$ MPa), the peak strengths decreased in the range of 1.93–37.78 MPa. Similarly, the peak strengths of the cubic granite specimens fluctuated

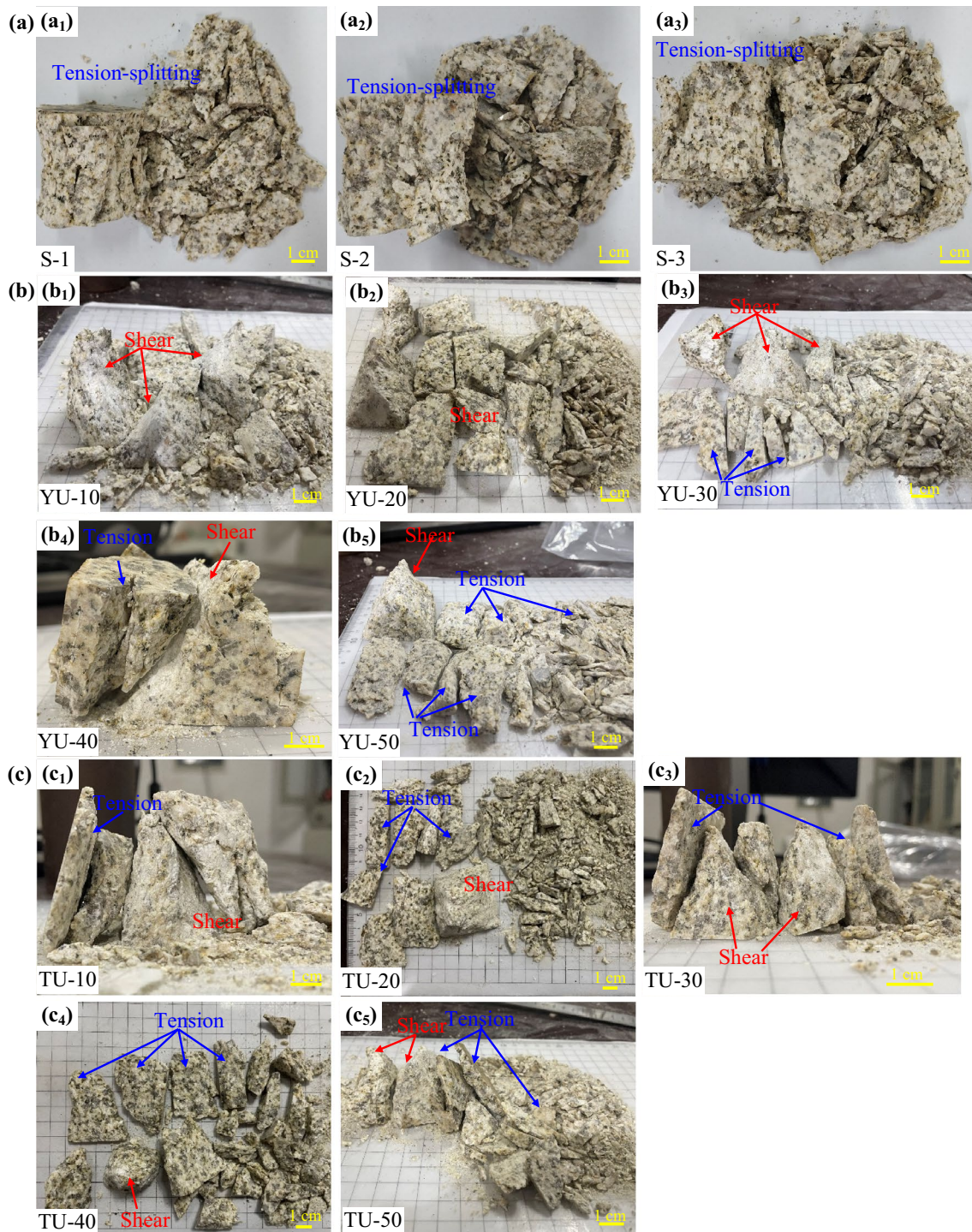


Fig. 10 Post-peak failure characteristics of specimens under **a** UC tests; **b** YU tests; **c** TU tests

from 137.48 to 87.60 MPa with increasing confining pressure in the TU tests, and the peak strengths decreased from 2.52 to 52.40 MPa. In addition, under the same confining

pressure, the peak strength of the granite in the TU test was lower than that in the YU test, and the stress difference between them increased with increase in the confining

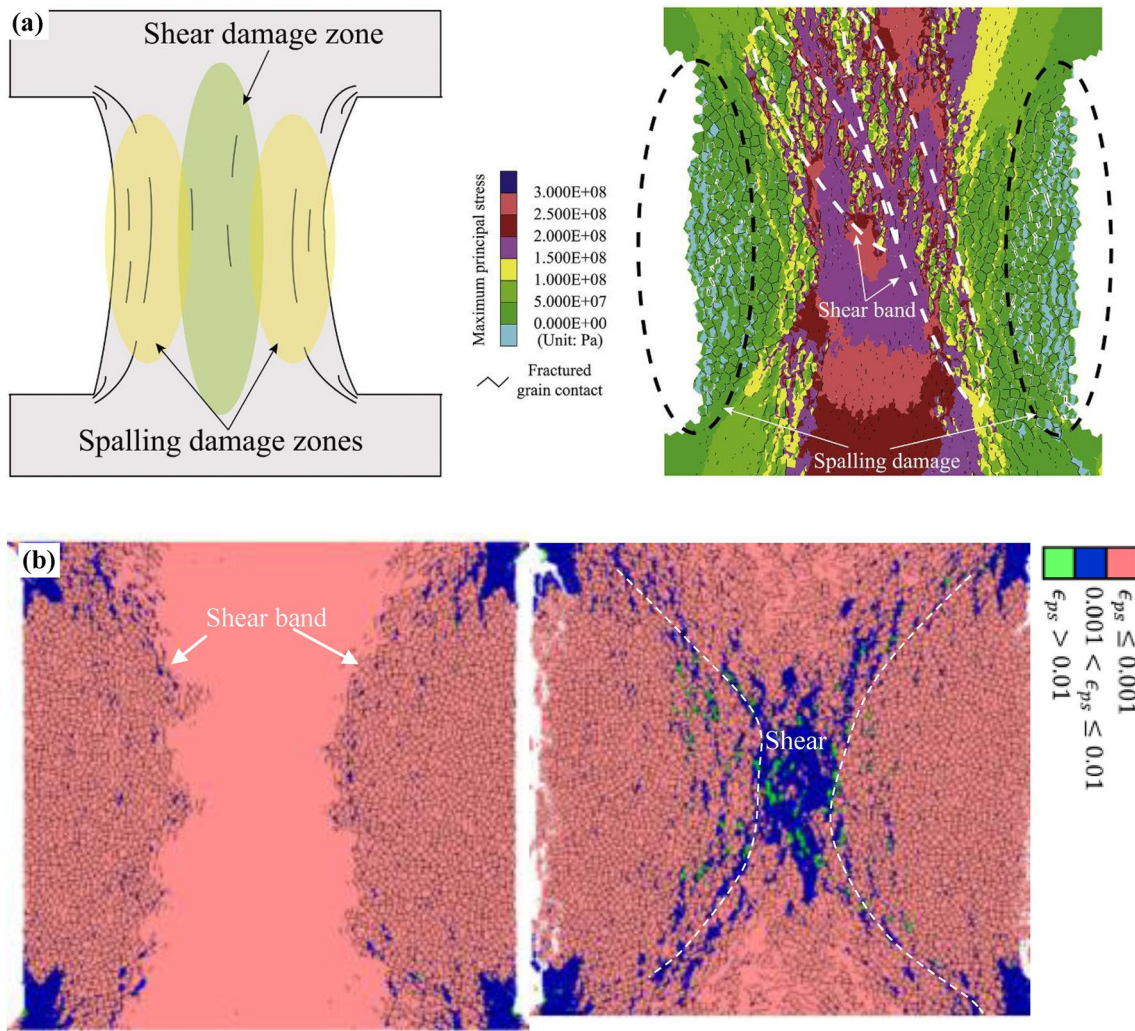


Fig. 11 Typical shear failure mode of rock pillar (Wang and Cai 2021; Sankhane and Walton 2018)

Table 2 Test results

Confining pressure	$\sigma_{\gamma U}$	σ_{TU}	$\sigma_{\gamma U}-\sigma_{TU}$	$UCS-\sigma_{\gamma U}$	$UCS-\sigma_{TU}$	SWR of $\sigma_{\gamma U}$	SWR of σ_{TU}	$(\sigma_{\gamma U}-\sigma_{TU})/\sigma_{\gamma U}$
(MPa)	(MPa)	(MPa)	(MPa)	(MPa)	(MPa)	(%)	(%)	(%)
0	140.00	140.00	0.00	0.00	0.00	0.00	0.00	0.00
10	138.07	137.48	0.59	1.93	2.52	1.38	1.80	0.43
20	135.60	133.20	2.40	4.40	6.80	3.14	4.86	1.77
30	124.17	120.40	3.77	15.83	19.60	11.31	14.00	3.04
40	113.29	104.36	8.93	26.71	35.64	19.08	25.46	7.88
50	102.22	87.60	14.62	37.78	52.40	26.99	37.43	14.30

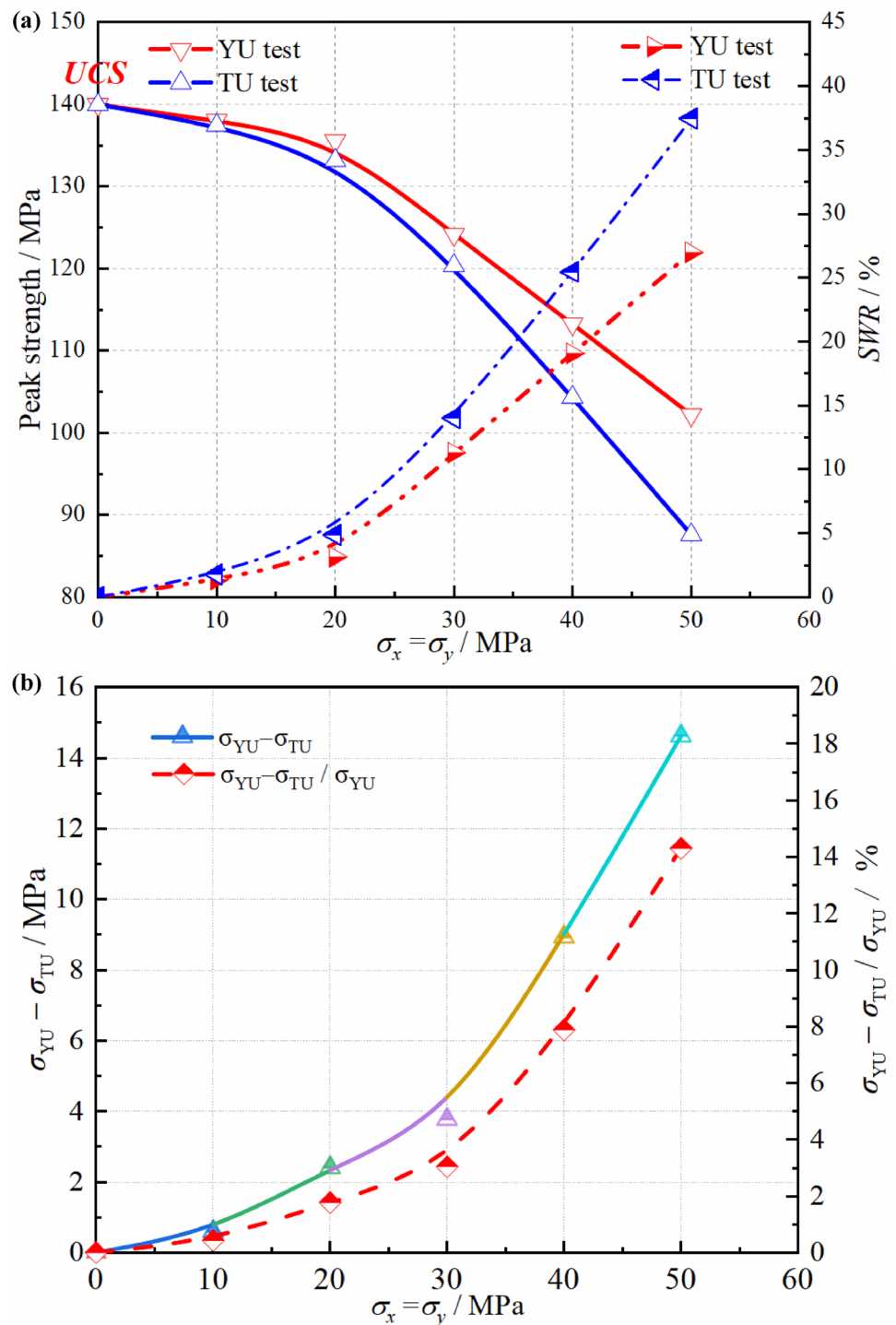
pressure. These trends suggest that the triaxial unloading path has a significant effect on the strength-reduction degree of a rock pillar.

To quantitatively express the strength-reduction effect of a rock pillar, the strength-weakening rate (SWR) is

proposed to characterize the strength-reduction degree as (Si and Gong 2020; Wu et al. 2022):

$$SWR = \frac{UCS - \sigma_i}{UCS} \times 100\%, \tag{1}$$

Fig. 12 Strength variation characteristics: **a** relationship between peak strength and confining pressure; **b** peak strength difference of granite specimens in TU and YU tests at same confining pressure

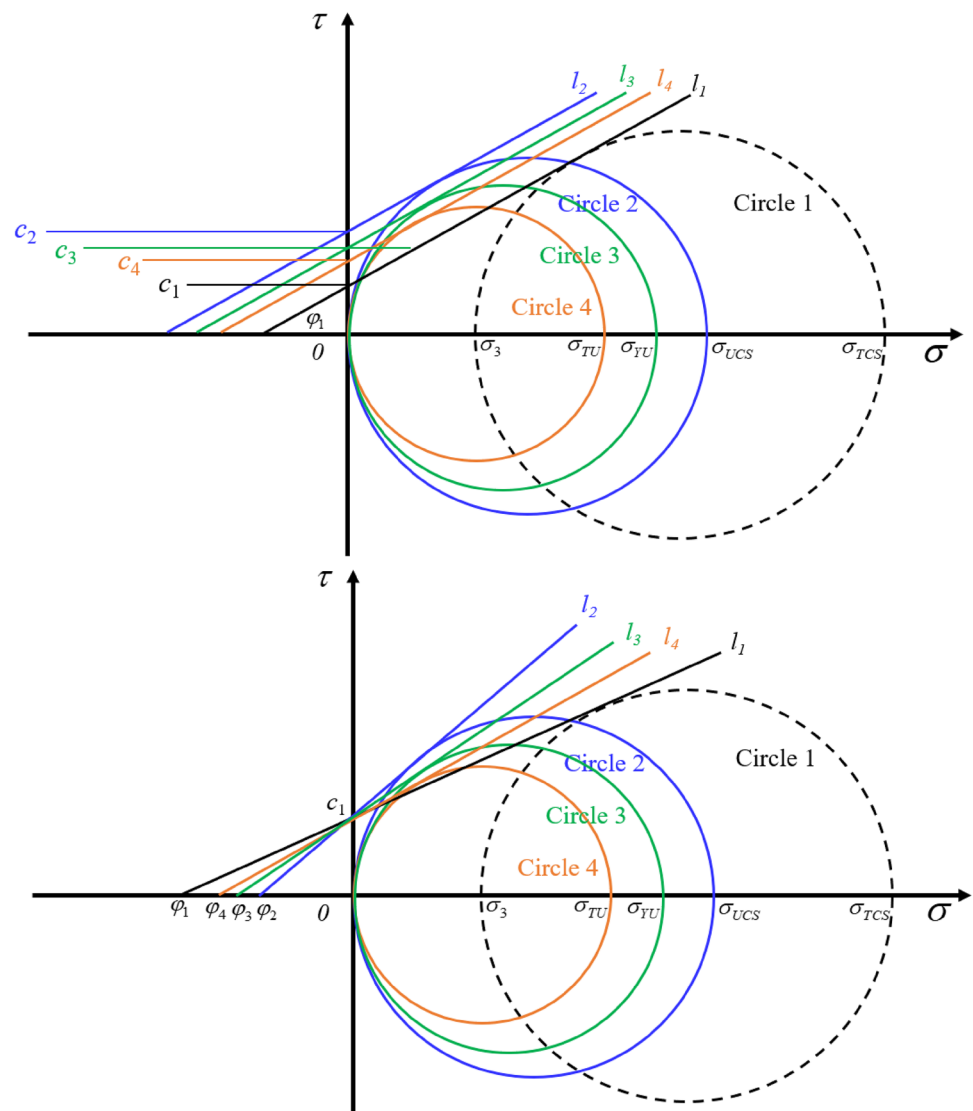


where UCS is the uniaxial compressive strength and σ_i is the peak strength in the YU or TU test under a particular confining pressure, $i = YU, TU$ test.

The SWR values under two triaxial unloading paths are listed in Table 2. Figure 12a reveals the relationship between the SWR and the confining pressure, i.e., the strength-reduction degree of the cubic granite specimen increases with increasing unloading confining pressure. The SWR values

from the TU tests were significantly higher than those from the YU tests, which indicates that the reduction degree of the peak strength by the simultaneous unloading stress path is larger than that by the sequential unloading stress path. Moreover, the peak strength difference between two triaxial unloading paths increased with increasing unloading confining pressure, as shown in Fig. 12b.

Fig. 13 Mohr–Coulomb stress circles under four different stress conditions



These trends suggest that high-stress unloading induces rock pillar strength reduction, and the triaxial unloading path affects its weakening intensity. Therefore, the strength-reduction effect of a rock pillar can be summarized as follows. First, the excavation-unloading process changes the stress state of the surrounding rock from a 3D stress state to a 1D stress state, which causes the rock pillar strength to sharply decrease. This is the dominant factor and inevitable. The strength-reduction effect induced by bidirectional simultaneous unloading is more significant than that by sequential unloading. When the bidirectional simultaneous excavation-unloading method is adopted for the construction of underground engineering, the stress adjustment rate of the surrounding rock is higher than when the bidirectional sequential unloading method is used. Therefore, the stress concentration is more significant in the former case, which makes the surrounding rock more prone to induce damage. As the excavation-unloading path is controllable during the

excavation process, the strength-reduction degree can be adjusted in this part.

Compared with the stress–strain curves and tension-splitting failure modes of the cubic granite specimens in pure UC tests, those in triaxial unloading path show a remarkable yield stage, and shear failure is the main failure mode (Figs. 7 and 10). In addition, the peak strengths of the cubic granite specimens under triaxial unloading paths show a notable strength-reduction effect. These results indicate that triaxial unloading affects the rock strength parameters. Generally, shear failure characteristics of rock materials can be described well by the Mohr–Coulomb strength criterion. This strength criterion is composed primarily of cohesion c and internal friction angle φ variation with the normal stress, i.e., $t = c + \tan \varphi$. The triaxial compress strength of a rock (σ_{TUS}) is typically higher than pure UC (σ_{UCS}). Accordingly, Mohr–Coulomb stress circles under four different stress conditions are shown in Fig. 13, wherein circles 1–4 represent

the triaxial compression, UC, YU, and TU tests, respectively. In this study, changes in strength parameters (c and φ) with the Mohr–Coulomb stress circles were examined to analyze the influence of triaxial unloading path, as follows. (1) It is assumed that φ_1 of a rock under loading and unloading conditions remains unchanged. The variation characteristics of c after 2D stress unloading are: $c_3 > c_4 > c_1$, i.e., the cohesion of a rock increases under confining pressure unloading. (2) It is assumed that c_1 of a rock under loading and unloading conditions remains unchanged. The variation characteristics of φ_1 after confining pressure unloading are as follows: $\varphi_3 > \varphi_4 > \varphi_1$, i.e., the internal friction angle of a rock increases under confining pressure unloading. (3) Compared with a UC test, after confining pressure unloading, c or φ decreases. This suggests that confining pressure unloading affects the strength parameters of rock. However, we did not examine the specific influence of unloading on the strength parameters (c and φ) and the constitutive relationship, and this will be the focus of our future research.

4 Discussion

4.1 Pillar Strength-Reduction Mechanism Under Triaxial High-Stress Unloading Path

In this study, the strength-reduction effect of a rock pillar was reproduced from the perspective of triaxial unloading path (i.e., 3D initial high stress + 2D stress unloading + 1D stress adjustment). Moreover, the strength-reduction effect of a rock pillar was attributed to the 3D initial stress and the 2D stress unloading path. Compared with a pure UC test, under a high-stress path, the cubic granite specimens experienced a 3D initial high stress and 2D stress unloading process. Triaxial unloading under different confining pressures induces rock local damage, thereby reducing its bearing capacity (Huang and Li 2014; Xu et al. 2019; Cai 2008a, b; Li et al. 2014; Martino and Chandler 2004). Moreover, it can be seen from Fig. 7 that the stress step will appear in the axial direction after unloading, indicating that the axial strain is increasing, which further indicates that the triaxial unloading causes damage to the rock, so the rock is more prone to failure. Therefore, the peak strengths in the triaxial unloading path tests were lower than those in the pure UC tests. When the confining pressure reached 50 MPa, the yield stage under high-confining pressure unloading gradually were very significant (Fig. 7). This is because after triaxial unloading under a high confining pressure, a wide damage zone appears in the surrounding rock, which results in numerous microcracks (Yan et al. 2011, 2015). Compared with the splitting failure mode of the cubic granite specimens under pure UC (Fig. 10a), those under triaxial unloading path are shear and shear–tension failure modes (Fig. 10b

and c). Furthermore, the peak strengths of the cubic granite specimens under high-confining pressure unloading were significantly lower than those under low-confining pressure unloading, regardless of the triaxial unloading stress path (Fig. 12). These results show that high-confining pressure unloading may change the rock properties (such as reduce the plastic-enhanced brittleness, as shown in Figs. 7 and 13), thus changing the failure mode of the rock and reducing both the peak strength and rockburst intensity. This also reflects that the 3D initial stress determines the strength-reduction level of a rock pillar. Second, the peak strengths of the cubic granite specimens in the TU tests were significantly lower than those in the YU tests, which indicates that the 2D stress unloading path affects the weakening intensity (Fig. 12b). In the TU tests, the X - and Y -directions were unloaded to 0 MPa simultaneously; therefore, the stress release was faster and the rock local damage was more severe. In the YU tests, the X - and Y -directions were unloaded to 0 MPa successively, i.e., the Y -direction stress remained unchanged, whereas the X -direction stress was reduced to 0 MPa. In these tests, the lateral stress suppresses the rock local damage. Thus, the peak strength of a rock pillar under simultaneous unloading is lower than that under sequential unloading, which indicates that the triaxial unloading path affects its weakening intensity.

In conclusion, the strength-reduction mechanism of a rock pillar under a high-stress path can be summarized as follows. The 3D initial stress determines the strength reduction level of the pillar, whereas the triaxial high-stress unloading induces a strength reduction effect and the unloading path affects its weakening intensity.

4.2 Engineering Significance of Considering the Rock Pillar Strength Reduction

Pillars are used in deep and high-stress mines to maintain the stability and integrity of openings (Cording et al. 2015; Renani and Martin 2018; Wang and Cai 2021). The design and construction of rock pillar in traditional deep mining engineering are basically based on the mechanical properties of rock under pure uniaxial compression. However, one aspect rarely considered in the analysis of rock pillar strength, is the influence of the stress path imposed on the pillar due to the excavation-unloading sequence of the pillars. This article presents a study of pillar strength from the perspective of 3D initial high stress + 2D stress unloading + 1D stress adjustment by simulating laboratory-scale rock specimens with a pillar structure. Our test results reveal that the initial high stresses unloading reduce the pillar strength and induces the strength reduction effect (Fig. 12). Further, the pillar strength under the simultaneous unloading path is lower than that under the sequential unloading

path (Fig. 12b). In this case, it seems hazardous to adopt the pillar strength under pure static loading as the sole reference for deep mine engineering design. Therefore, for the safe construction and operation of deep mining engineering, it is necessary to establish a new design and construction standard considering the excavation-unloading effect, wherein necessary to measure the initial high stresses, determine the unloading path, and even the unloading rate adopted, and the possible reduction degree of the pillar strength induced by unloading should be pre-estimated.

Size effects also have a significant influence on the results of the pillar models. In this study, we used the original rock for the test and the failure and strength characteristics of rock pillars were studied under triaxial unloading paths of 3D initial high stress followed by 2D stress unloading and 1D stress adjustment. Although the results of laboratory-scale rock pillar model test simulation are similar to those of on-site deep mining engineering, can provide some insights for pillar design and hazard prevention in deep mines, it is hard to up-scale the laboratory-scale pillar model size to a full-size pillar model on-site. Thus, this study only conducts qualitative analysis. Future research is needed to address these challenging issues.

5 Conclusions

In this study, a series of simulated pillar rockburst and strength characteristics tests under a “3D initial high stress + 2D stress unloading + 1D stress adjustment” stress path were considered from the perspective of an entire stress path. Their results were compared to those obtained in pure UC tests. The effects of triaxial high-stress unloading paths on the mechanical and failure characteristics of cubic granite specimens were examined in detail, and the main conclusions were as follows.

- (1) Strength-reduction effect of rock pillar under triaxial high-stress unloading path. The compressive strength under triaxial unloading was significantly lower than the *UCS*, which indicates a notable strength-reduction effect. *SWR* was proposed to represent the characteristics of the strength reduction. It was found that the *SWR* increased significantly with increase in the confining pressure, thus indicating that a high-confining pressure during triaxial unloading implies a significant strength-reduction degree.
- (2) The triaxial unloading path has a significant influence on the rock pillar strength-reduction effect. The peak strength in the horizontal bidirectional sequential unloading was higher than that in the horizontal bidirectional simultaneous unloading. The peak strength difference increased gradually with increasing confin-

ing pressure, and the maximum difference observed was 14.62 MPa. In addition, the *SWR* values were approximately 26.99% and 37.43% under the horizontal bidirectional sequential and simultaneous unloading, respectively. These results indicate that the unloading path affects the weakening intensity.

- (3) Violent rockburst occurred in all specimens, and the deep rock pillar strength-reduction mechanism is summarized as follows. The 3D initial stress determines the strength-reduction level of the rock pillar, whereas the triaxial high-stress unloading induces a strength-reduction effect, and the specific unloading path affects its weakening intensity.

Acknowledgements This work was supported by the National Natural Science Foundation of China (Grant No. 42077244), the Open Research Fund of State Key Laboratory of Geomechanics and Geotechnical Engineering, Institute of Rock and Soil Mechanics, Chinese Academy of Sciences (Grant No. Z020005) and the Fundamental Research Funds for the Central Universities (Grant No. 2242022k30054). Many thanks to Mr. Jifu Gao, the general manager of Jing-cheng Geotechnical Service Company which locates in Liu-yang City, Hunan Province of China, for his sincere help in processing rock specimens. The authors would like to express appreciation to the reviewers for their valuable comments and suggestions that helped improve the quality of our paper.

Data Availability All data, models, or codes that support the findings of this study are available from the corresponding author (feng-qianguang@126.com) upon reasonable request.

Declarations

Conflict of Interest We would like to declare that the work described is original research that has not been published previously, and is not under consideration for publication elsewhere, in whole or in part. We declare that we do not have any commercial or associative interest that represents a conflict of interest in connection with the work submitted. The manuscript is approved by all authors for publication.

References

- Cai M (2008a) Influence of stress path on tunnel excavation response—Numerical tool selection and modelling strategy. *Tunn Undergr Space Technol* 23:618–628. <https://doi.org/10.1016/j.tust.2007.11.005>
- Cai M (2008b) Influence of intermediate principal stress on rock fracturing and strength near excavation boundaries—Insight from numerical modelling. *Int J Rock Mech Min Sci* 45:763–772. <https://doi.org/10.1016/j.ijrmms.2007.07.026>
- Chen SL, Lee SC, Cui MW (2009) Effects of rock pillar width on the excavation behavior of parallel tunnels. *Tunn Undergr Space Technol* 24:148–154. <https://doi.org/10.1016/j.tust.2008.05.006>
- Cording EJ, Hashas YMA, Oh J (2015) Analysis of pillar stability of mined gas storage caverns in shale formations. *Eng Geol* 184:71–80. <https://doi.org/10.1016/j.enggeo.2014.11.001>
- Deng J (2021) Analytical and numerical investigations on pillar rockbursts induced by triangular blasting waves. *Int J Rock Mech Min Sci* 138:104518. <https://doi.org/10.1016/j.ijrmms.2020.104518>

- Deng J, Kanwar NS, Pandey MD, Xie WC (2019) Dynamic buckling mechanism of pillar rockbursts induced by stress waves. *J Rock Mech Geotech Eng* 11:944–953. <https://doi.org/10.1016/j.jrmge.2019.02.005>
- Esterhuizen GS, Dolinar DR, Ellenberger JL (2011) Pillar strength in underground stone mines in the United States. *Int J Rock Mech Min Sci* 48:42–50. <https://doi.org/10.1016/j.ijrmmms.2010.06.003>
- Esterhuizen G (2006) An evaluation of the strength of slender pillars. *Trans Soc Min Metall Explor* 320:69–76
- Feng XT, Haimson B, Li XC et al (2019) ISRM Suggested Method: Determining deformation and failure characteristics of rocks subjected to true triaxial compression. *Rock Mech Rock Eng* 52:2011–2020. <https://doi.org/10.1007/s00603-019-01782-z>
- Gong FQ, Li XB, Li XL, Zhao J (2010) Experimental study of dynamic characteristics of sandstone under one-dimensional coupled static and dynamic loads. *Chin J Rock Mech Eng* 29(10):2076–2085
- Gong FQ, Luo Y, Li XB, Si XF, Tao M (2018) Experimental simulation investigation on rockburst induced by spalling failure in deep circular tunnels. *Tunn Undergr Space Technol* 81:413–427. <https://doi.org/10.1016/j.tust.2018.07.035>
- Gong FQ, Wu WX, Ren L (2023) Rockburst process and strength-weakening effect of the high-stress circular tunnel under internal unloading. *J Rock Mech Geotech Eng*. <https://doi.org/10.1016/j.jrmge.2022.10.016>
- He MC, Liu DQ, Gong WL et al (2014) Development of a testing system for impact rockbursts. *Chin J Rock Mech Eng* 33(9):1729–1739
- He MC, Ren FQ, Liu DQ, Zhang S (2021) Experimental Study on strain burst characteristics of sandstone under true triaxial loading and double faces unloading in one direction. *Rock Mech Rock Eng* 54:149–171. <https://doi.org/10.1007/s00603-020-02272-3>
- Hu XC, Su GS, Chen GY, Mei SM, Feng XT, Mei GX, Huang XH (2019) Experiment on rockburst process of borehole and its acoustic emission characteristics. *Rock Mech Rock Eng* 52:783–802. <https://doi.org/10.1016/j.ijrmmms.2009.09.003>
- Huang D, Li YR (2014) Conversion of strain energy in triaxial unloading tests on marble. *Int J Rock Mech Min Sci* 66:160–168. <https://doi.org/10.1016/j.ijrmmms.2013.12.001>
- Huang HX, Li J, Jiang H (2017) Theoretical derivation of basic mechanical property required for triggering mine-pillar rockburst. *Acta Geophys* 65:945–955. <https://doi.org/10.1007/s11600-017-0081-2>
- Jiang Q, Zhang MZ, Yan F, Su G, Feng G (2021) Effect of initial minimum principal stress and unloading rate on the spalling and rockburst of marble: a true triaxial experiment investigation. *Bul Eng Geo Envir* 80:1617–1634. <https://doi.org/10.1007/s10064-020-01995-5>
- Kaiser PK, Kim B, Bewick RP, Valley B (2011) Rock mass strength at depth and implications for pillar design. *Min Tech* 120(3):170–179. <https://doi.org/10.1179/037178411X12942393517336>
- Kate O, Reches Z (2004) Microfracturing, damage, and failure of brittle granites. *J Geophys Res* 109:B01206. <https://doi.org/10.1029/2002JB001961>
- Li CL (2021) Principles and methods of rock support for rockburst control. *J Rock Mech Geotech Eng* 13:46–59. <https://doi.org/10.1016/j.jrmge.2020.11.001>
- Li XB, Li DY, Guo L, Ye ZY (2007) Study on mechanical response of highly-stressed pillars in deep mining under dynamic disturbance. *Chin J Rock Mech Eng* 26(5):922–928. [https://doi.org/10.1016/S1872-2067\(07\)60020-5](https://doi.org/10.1016/S1872-2067(07)60020-5)
- Li XB, Cao WZ, Zhou ZL, Zou Y (2014) Influence of stress path on excavation unloading response. *Tunn Undergr Space Technol* 42:237–246. <https://doi.org/10.1016/j.tust.2014.03.002>
- Li XB, Gong FQ, Tao M, Dong LJ, Du K, Ma CD, Zhou ZL, Yin TB (2017) Failure mechanism and coupled static-dynamic loading theory in deep hard rock mining: a review. *J Rock Mech Geotech Eng* 9(4):767–782. <https://doi.org/10.1016/j.jrmge.2017.04.004>
- Li XY, Kim EH, Walton G (2019) A study of rock pillar behaviors in laboratory and in-situ scales using combined finite-discrete element method models. *Int J Rock Mech Min Sci* 118:21–32. <https://doi.org/10.1016/j.ijrmmms.2019.03.030>
- Liu DQ, Ling K, Li D, He MC, Li JY, Han ZJ, Zhang SD (2021) Evolution of anisotropy during sandstone rockburst process under double-faces unloading. *J Cent South Univ* 28(8):2472–2484. <https://doi.org/10.1007/s11771-021-4780-0>
- Luo Y, Gong FQ, Dong-qiao LIU, Si XF (2019) Experimental simulation analysis of the process and failure characteristics of spalling in D-shaped tunnels under true-triaxial loading conditions. *Tunn Undergr Space Technol* 90:42–61. <https://doi.org/10.1016/j.tust.2019.04.020>
- Martin CD (1997) Seventeenth Canadian geotechnical colloquium: the effect of cohesion loss and stress path on brittle rock strength. *Can Geotech J* 34(5):698–725. <https://doi.org/10.1139/cgj-34-5-698>
- Martin CD, Maybee WG (2000) The strength of hard-rock pillars. *Int J Rock Mech Min Sci* 37:1239–1246. [https://doi.org/10.1016/S1365-1609\(00\)00032-0](https://doi.org/10.1016/S1365-1609(00)00032-0)
- Martin CD, Kaise PK, Christiansson R (2003) Stress, instability and design of underground excavations. *Int J Rock Mech Min Sci* 40:1027–1047. [https://doi.org/10.1016/S1365-1609\(03\)00110-2](https://doi.org/10.1016/S1365-1609(03)00110-2)
- Martino JB, Chandler NA (2004) Excavation-induced damage studies at the Underground Research Laboratory. *Int J Rock Mech Min Sci* 41(8):1413–1426. <https://doi.org/10.1016/j.ijrmmms.2004.09.010>
- Ortlepp WD, Stacey TR (1994) Rockburst mechanisms in tunnels and shafts. *Tunn Undergr Space Technol* 9(1):59–65. [https://doi.org/10.1016/0886-7798\(94\)90010-8](https://doi.org/10.1016/0886-7798(94)90010-8)
- Renani HR, Martin CD (2018) Modeling the progressive failure of hard rock pillars. *Tunn Undergr Space Technol* 74:71–81. <https://doi.org/10.1016/j.tust.2018.01.006>
- Sankhanee LS, Walton G (2018) A progressive S-shaped yield criterion and its application to rock pillar behavior. *Int J Rock Mech Min Sci* 105:98–109. <https://doi.org/10.1016/j.ijrmmms.2018.03.014>
- Sengani F (2018) The performance of bolt-reinforced and shotcreted in-stope pillar in rockburst-prone areas. *Int J Min Geo-Eng* 52(2):105–117. <https://doi.org/10.22059/ijmge.2018.251957.594715>
- Si XF, Gong FQ (2020) Strength-weakening effect and shear-tension failure mode transformation mechanism of rockburst for fine-grained granite under triaxial unloading compression. *Int J Rock Mech Min Sci* 131:104347. <https://doi.org/10.1016/j.ijrmmms.2020.104347>
- Sinha S, Walton G (2021a) Investigation of pillar damage mechanisms and rock-support interaction using Bonded Block Models. *Int J Rock Mech Min Sci*. <https://doi.org/10.1016/j.ijrmmms.2021a.104652>
- Sinha S, Walton G (2021b) Integration of three-dimensional continuum model and two-dimensional bonded block model for studying the damage process in a granite pillar at the Creighton Mine, Sudbury, Canada. *J Rock Mech Geotech Eng* 13:275–288. <https://doi.org/10.1016/j.jrmge.2020.06.011>
- Wang MZ, Cai M (2021) Numerical modeling of time-dependent spalling of rock pillars. *Int J Rock Mech Min Sci* 141:104725. <https://doi.org/10.1016/j.ijrmmms.2021.104725>
- Wu WX, Gong FQ, Yang WM (2020) Experimental simulation study of spalling in deep rectangular tunnel with plastic fine grain marble. *Tunn Undergr Space Technol* 98:103319. <https://doi.org/10.1016/j.tust.2020.103319>
- Wu WX, Gong FQ, Jiang Q (2022) Strength weakening effect of high static pre-stressed granite subjected to low-frequency dynamic disturbance under uniaxial compression. *Trans Nonferrous Met*

- Soc China 32(7):2353–2369. [https://doi.org/10.1016/S1003-6326\(22\)65952-1](https://doi.org/10.1016/S1003-6326(22)65952-1)
- Xu S, Liu JP, Xu SD, Wei J, Huang WB, Dong LB (2012) Experimental studies on pillar failure characteristics based on acoustic emission location technique. *Trans Nonferrous Metals Soc China* 22:2792–2798. [https://doi.org/10.1016/S1003-6326\(11\)61534-3](https://doi.org/10.1016/S1003-6326(11)61534-3)
- Xu H, Feng XT, Yang CX, Zhang XW, Zhou YY, Wang ZF (2019) Influence of initial stresses and unloading rates on the deformation and failure mechanism of Jinping marble under true triaxial compression. *Int J Rock Mech Min Sci* 117:90–104. <https://doi.org/10.1016/j.ijrmms.2019.03.013>
- Yan P, Lu WB, Chen M, Shan ZG, Chen XR (2011) In-situ test research on influence of excavation method on induced damage zone in deep tunnel. *Chin J Rock Mech Eng* 30(6):1097–1106. <https://doi.org/10.1111/j.1553-2712.1995.tb03289.x>
- Yan P, Zhao ZG, Lu WB, Fan Y, Chen XR, Shan ZG (2015) Mitigation of rock burst events by blasting techniques during deep-tunnel excavation. *Eng Geol* 188:126–136. <https://doi.org/10.1016/j.enggeo.2015.01.011>
- Zhang CQ, Feng XT, Zhou H, Qiu SL, Wu WQ (2012) Case histories of four extremely intense rockbursts in deep tunnels. *Rock Mech Rock Eng* 45:275–288. <https://doi.org/10.1007/s00603-011-0218-6>
- Zhao XG, Cai M (2015) Influence of specimen height-to-width ratio on the strainburst characteristics of Tianhu granite under true-triaxial unloading conditions. *Can Geotech J* 52(7):890–902. <https://doi.org/10.1139/cgj-2014-0355>

Publisher's Note Springer Nature remains neutral with regard to jurisdictional claims in published maps and institutional affiliations.

Springer Nature or its licensor (e.g. a society or other partner) holds exclusive rights to this article under a publishing agreement with the author(s) or other rightsholder(s); author self-archiving of the accepted manuscript version of this article is solely governed by the terms of such publishing agreement and applicable law.